Macromolecules

Article

pubs.acs.org/Macromolecules

Multiresponsive Microcapsules Based on Multilayer Assembly of Star Polyelectrolytes

Weinan Xu,[†] Petr A. Ledin,[†] Felix A. Plamper,[‡] Christopher V. Synatschke,[‡] Axel H. E. Müller,[‡] and Vladimir V. Tsukruk*,[†]

[†]School of Materials Science and Engineering, Georgia Institute of Technology, Atlanta, Georgia 30332, United States

[‡]Makromolekulare Chemie II and Bayreuther Zentrum fur Kolloide und Grenzflächen, Universitat Bayreuth, D-95440 Bayreuth, Germany

Supporting Information

ABSTRACT: Star polyelectrolytes (poly(*N*,*N*-dimethylaminoethyl methacrylate) (PDMAEMA)) with dual (temperature and pH) responsive properties were utilized to fabricate multiresponsive microcapsules via layer-by-layer (LbL) assembly. The LbL microcapsules are very robust and uniform, with higher stability and different internal structure compared with conventional microcapsules based on linear polyelectrolytes. Ionic strength in the polyelectrolyte solution during the microcapsule assembly process has a significant influence on the thickness and permeability of microcapsules. With increasing pH, the permeability of microcapsules decreases, and the transition from "open" to "closed" state for target molecules can be achieved within a narrow pH range (from pH 7 to 8). On the other hand, the overall size and permeability of the microcapsules decrease with increasing temperature (with a shrinkage of 54% in diameter at 60 °C compared with room temperature), thus allowing to reversibly load and unload the microcapsules with high efficiency. The organization and interaction of star polyelectrolytes within confined multilayer structure are the main driving forces for the responsiveness to external stimuli. The multiresponsive LbL microcapsules represent a novel category of smart microstructures as compared to traditional LbL microcapsules with "one-dimensional" response to a single stimulus, and they also have the potential to mimic the complex responsive microstructures found in nature and find applications in drug delivery, smart coatings, microreactors, and biosensors.

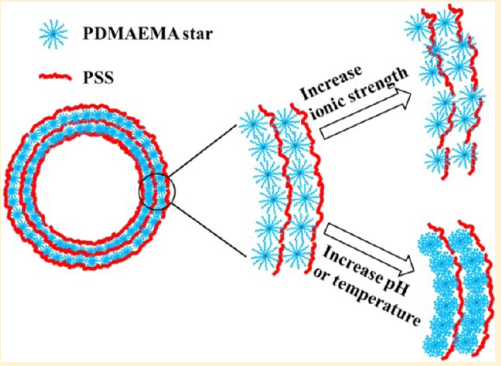

1. INTRODUCTION

Stimuli-responsive polymeric structures have attracted much attention in recent years due to their diverse range of potential applications.[1] There are many different categories of responsive polymeric structures, such as brushes,[2] thin films,[3] micro- and nanogels,[4] micelles,[5,6] hybrid particles,[7,8] nanotubes,[9] microcapsules,[10] biomaterial sheets,[11] and thin shells for cells.[12,13] Among these different materials, responsive microcapsules have their unique and superior properties, such as easy fabrication, high stability, high loading capacity, and controlled release of cargo molecules.[10,14] During the past decade, layer-by-layer (LbL) assembly has emerged to be an important tool to fabricate microcapsules because of its many advantages, such as high versatility, uniformity, broad choice of materials, and facile incorporation of multiple functionalities.[15−18]

LbL microcapsules and shells with stimuli-responsive properties have been studied intensively in recent years due to their emerging applications in drug delivery, tissue engineering, implantation, coatings, and biosensors.[19] Traditional stimuli used to modulate the structure and properties of LbL microcapsules include pH and ionic strength[20,21]—usually for microcapsules composed of weak polyelectrolytes, because the charge density and electrostatic interaction within the shell change with pH value, rendering their structure and permeability pH-responsive.[22] Because of the charge screening effect with the increasing ionic strength, the electrostatic interaction between oppositely charged polyelectrolytes decreases,[23] which leads to an increased permeability of the microcapsules with a polyelectrolyte multilayer shell.[24]

Besides pH and ionic strength, other environmental stimuli such as light,[25−27] magnetic or electric fields,[28,29] chemical stimuli,[30] ultrasound,[31] and temperature[32] are also highly attractive.[33] Generally, these stimuli can be remotely controlled and require only mild changes in the environment, making them more desirable in certain applications. Most of the previous work in this field is focused on responsiveness to a specific type of stimulus;[34] the integration of responsiveness to the novel stimuli with that to traditional stimuli (pH, ionic strength) has received little attention so far. On the other hand, in order to satisfy the requirements of some more demanding tasks,[35] and to have smart systems that can react to different stimuli at the desired location, condition, and time, the

Received: September 7, 2014
Revised: October 24, 2014
Published: November 10, 2014

   dx.doi.org/10.1021/ma501853c | Macromolecules 2014, 47, 7858−7868

Scheme 1. (a) Chemical Structure of PDMAEMA Star Polymers and (b) Assembly of $(PSS/PDMAEMA_{18})_n$ LbL Microcapsules

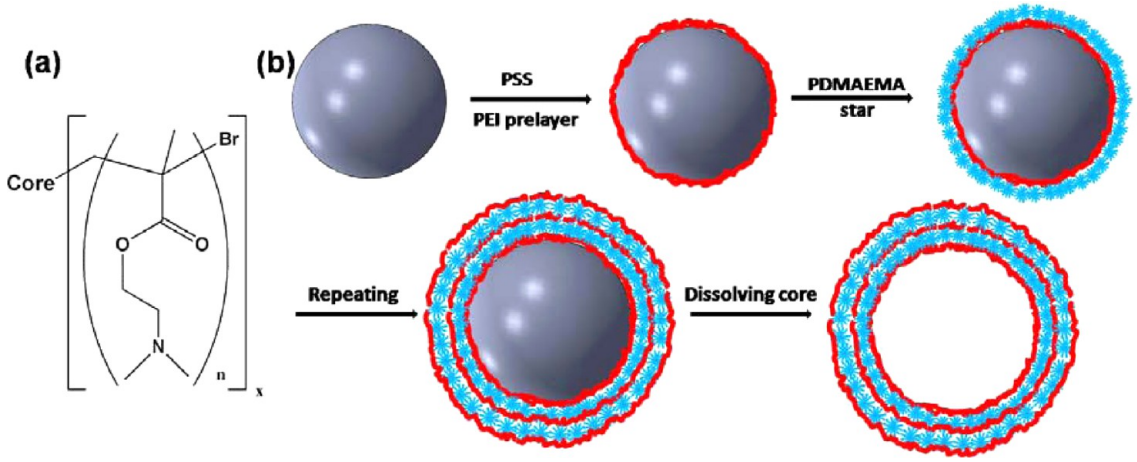

integration of multiresponsive properties into one single type of microcapsule is a very attractive option.[36] Moreover, in many practical applications the change in environment is often includes several interrelated factors, and a change in one factor often induces the variation of others. Therefore, the ability to respond to several external stimuli simultaneously or in orthogonal way is of significant interest.

Several previous reports describe multiresponsive microcapsules. For instance, Chu et al.[37] reported the temperature−magnetic field dual responsive microcapsules that rely on the incorporation of magnetic nanoparticles. Gao et al.[38] showed that by using the host−guest interaction, LbL microcapsules can possess multiresponsiveness to pH, ionic strength, and selectively binding molecules, but such host−guest interaction can only apply to limited specific molecules. Pich et al.[39] reported composite microcapsules with responsive microgel particles embedded in the shell, which respond to temperature and solvent concentration, but the responses take a long time. Despite the great potential of multiresponsive microcapsules, there are still many fundamental and practical issues to be addressed: for example, the role of polymer architecture in the responsiveness of polymeric microcapsules, the effects of organization and interaction of the building blocks within the microcapsule shell on their responsive properties, the potential interaction or crosstalk among different external stimuli, and precise morphological changes, which accompany apparent microcapsule variations.

For the purpose of fabricating multifunctional or multiresponsive microstructures, star polymers stand out as an excellent candidate material because they have the advantages of having multiple functionalities,[40] flexible compositions,[41] and unique responses caused by well-defined macromolecular segments.[42] Because of the unique branched architecture and peculiar intermolecular interactions of star polymers,[43] they can bring unique internal structure and significantly different physical properties to the fabricated microstructures including microcapsules.[44] For example, star-shaped polystyrene-*block*-poly(2-pyridine) (PS_nP2VP_n) block copolymers have been used to fabricate LbL microcapsules;[45] the prepared microcapsules have a multicompartmental shell structure with densely packed hydrophobic domains within the hydrophilic matrix. Poly{[2-(methacryloyloxy)ethyl]trimethylammonium iodide} (PMETAI) star polyelectrolytes have also been used in LbL assembly of microcapsules,[27] and due to the unique response of PMETAI stars to multivalent salt, the permeability of the microcapsules can be reversibly tuned by the counterion valency and UV irradiation. However, those previous studies on microcapsules with star polymer components have not demonstrated multiple responsive behaviors.

Herein, we utilize PDMAEMA star polyelectrolytes with dual response to pH and temperature to fabricate LbL microcapsules. PDMAEMA is a well-known water-soluble and stimuli-responsive polyelectrolyte with a wide range of applications.[46] As a weak polyelectrolyte, its charge density depends on the solution pH. With decreasing pH value, the ionization degree of the amino groups is higher; therefore, the polymer has a higher charge density, and previous studies showed that the $(PDMAEMA_{170})_{18}$ star polyelectrolyte has a pK_a of 5.8.[47] The prepared microcapsules based on PDMAEMA stars are very robust, and their structure and permeability are readily responsive to external stimuli such as pH, temperature, and ionic strength. The pH-controlled permeable−impermeable transition occurs in a very narrow pH range, which is superior to most previous reports.[48,49] Taking advantage of the thermoresponsive properties, a highly efficient and reversible loading−unloading patter under cross-correlated stimuli can be achieved.

2. RESULTS AND DISCUSSION

Fabrication of LbL Microcapsules. The star architecture provides many unique properties compared with the linear counterparts, and for the sake of comparison, both star and linear PDMAEMA were used as the polycations and poly(sodium 4-styrenesulfonate) (PSS) was used as the polyanion to fabricate LbL microcapsules via electrostatic interaction (Scheme 1). The LbL microcapsules are named $(PSS/PDMAEMA_{18})_n$ or $(PSS/PDMAEMA_1)_n$, where the subscript 18 refers to the PDMAEMA star with 18 arms, while the subscript 1 refers to linear PDMAEMA, and n indicates the number of bilayers.

The LbL assembly of PSS and PDMAEMA stars was conducted at pH 5 condition, since at this condition the PDMAEMA stars have higher charge content and the electrostatic interaction with anionic PSS is stronger, which is beneficial to the assembly process. The two polyelectrolyte components were dissolved in 0.1 M NaCl solution; due to the presence of salt, the charge on the polyelectrolyte backbones was partially screened, which has significant influence on the

dx.doi.org/10.1021/ma501853c | Macromolecules 2014, 47, 7858−7868

structure and permeability of the resulting hollow microcapsules, as will be discussed later.

Electrophoresis experiments were conducted to monitor the LbL growth of PSS and PDMAEMA star polyelectrolytes (Figure 1). The ζ-potential of bare silica particle at pH 5 buffer

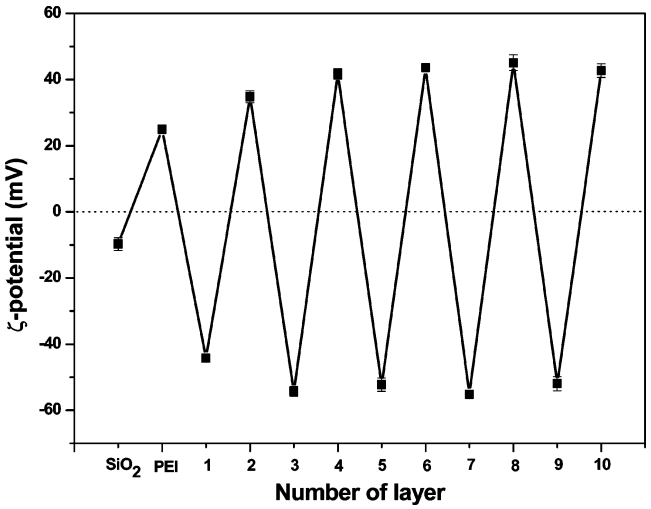

Figure 1. ζ-potential as a function of number of layers during LbL assembly on silica microparticles with alternating (PSS/PDMAEMA$_{18}$) bilayers.

was around −9.8 mV. A ζ-potential of ca. −52.0 mV was obtained for microcapsules when PSS was the outmost layer of film on silica core. On the other hand, a ζ-potential of ca. +42.7 mV was observed when PDMAEMA$_{18}$ star polyelectrolyte was the outmost layer. Overall, the alternating surface charge of coated silica particles serves as strong evidence that consistent assembly of anionic PSS and cationic PDMAEMA components took place during the fabrication process.[50,51]

Morphology of (PSS/PDMAEMA)$_n$ LbL Microcapsules. From the scanning electron microscope (SEM) images in Figure 2, it can be seen that the hollow microcapsules collapse after drying with formation of random wrinkles. With the increase of number of bilayers, the contact area of the collapsed microcapsules with the substrate decreases and wrinkles on the surface also become larger. Figure 3 shows representative transmission electron microscopy (TEM) images of (PSS/PDMAEMA$_{18}$)$_{11}$ microcapsules, where it can be seen clearly that the microcapsules are hollow without any residual core materials inside.

Further surface analysis was conducted using atomic force microscopy (AFM), as shown in Figure 4. The left column images show the whole microcapsules with increasing number of bilayer. From a smaller area scan depicted in the right column of Figure 4, it can be seen that the surface possesses a highly dense granular morphology, where the average size of individual granules (30−40 nm) matches dimensions of PDMAEMA stars (Figure S1).

The data on thickness of the microcapsules in dry state are summarized in Figure 4g. The thickness of the microcapsules increases significantly from 5 bilayers to 8 and 11 bilayers. In contrast, microcapsules from linear PDMAEMA and PSS have significantly thinner shell. It can also been seen from Figure 4 that with the increase of bilayer number, the number of wrinkles on the dried microcapsules decreases, while the

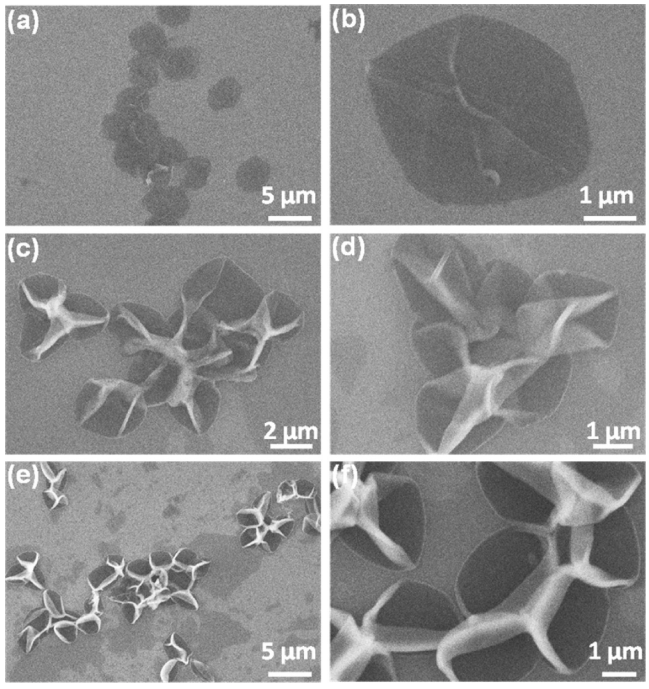

Figure 2. SEM images of (PSS/PDMAEMA$_{18}$)$_n$ microcapsules with different number of bilayers: (a, b) 5, (c, d) 8, (e, f) 11.

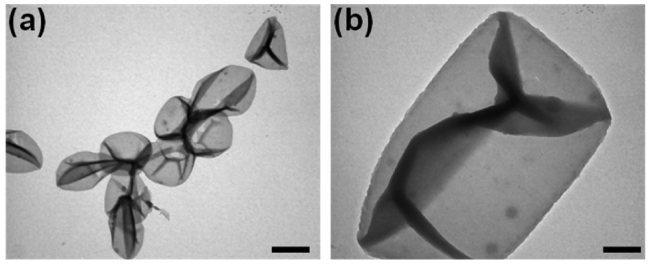

Figure 3. TEM images of (PSS/PDMAEMA$_{18}$)$_{11}$ microcapsules. The scale bar is 2 μm in (a) and 500 nm in (b).

wrinkles become larger; some of them cover almost half of the whole collapsed microcapsules.

The main reason for thicker shell of (PSS/PDMAEMA$_{18}$)$_n$ microcapsule is that star PDMAEMA has more abundant functional groups and chain ends; therefore, their electrostatic interaction with PSS is stronger, and the amount of adsorbed polyelectrolytes in each layer on the silica core is more than that of microcapsules from linear PDMAEMA. On the other hand, the thicker shell of the star PDMAEMA-based microcapsules leads to better mechanical stability; the shell becomes more rigid and less easy to deform, which allows the microcapsules to be persistent against local capillary forces during the drying process.[45] As a result, the microcapsules only partially collapse, with a large wrinkle on the surface (Figure 4c,e). On the contrary, (PSS/PDMAEMA$_1$)$_n$ microcapsules with lower mechanical stability collapse completely on the substrate, and the contact area of the microcapsules remains almost the same for different bilayer numbers (Figure S2).

Effects of Ionic Strength and Polymer Architecture on Microcapsule Behavior. We found a significant influence of the ionic strength of the solution used to prepare the microcapsules on their properties. To study this effect, we used two different polyelectrolyte solutions: one with 0.2 mg/mL polyelectrolytes dissolved in 0.1 M NaCl solution with

dx.doi.org/10.1021/ma501853c | Macromolecules 2014, 47, 7858−7868

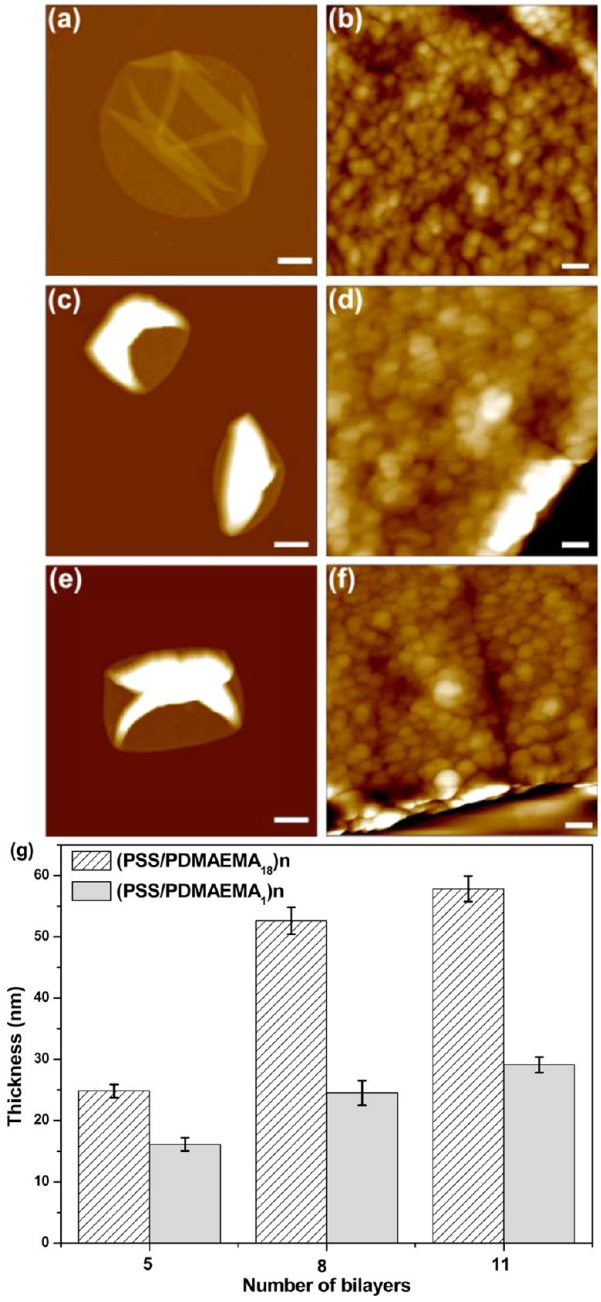

Figure 4. AFM images of $(PSS/PDMAEMA_{18})_n$ microcapsule with 5 bilayers (a, b), 8 bilayers (c, d), and 11 bilayers (e, f). The *Z* range is 1500 nm (a, c, e) and 50 nm (b, d, f); scale bar is 1 μm (a, c, e) and 100 nm (b, d, f). (g) Thickness comparison of microcapsules with different bilayer numbers.

adjusted pH and the other with 0.2 mg/mL polyelectrolytes dissolved in pure water with adjusted pH. It is worth to mention that all microcapsules, regardless of which solution was used for their preparation, were dialyzed in pure water after core dissolution. This procedure should remove almost all of the excess ions even from the LBL multilayers, leading to a "frozen" structure of the shell, which is cross-linked by electrostatic interaction and remains stable when exposed to salt-free condition afterward.

The microcapsule permeability was measured by using fluorescein isothiocyanate (FITC) or FITC-labeled dextrans of various molecular weights as fluorescent probes in 0.01 M Tris-HCl buffer with adjusted pH. If the pore size of the microcapsules shell is larger than the size of the fluorescent probe, then the fluorescent intensity would be almost the same for the interior and exterior of the microcapsules; otherwise, the interior would be dark and the background appears bright. The $(PSS/PDMAEMA_{18})$ microcapsules have quite low permeability; as shown in Figure 5, FITC-dextran with M_w of 4 kDa

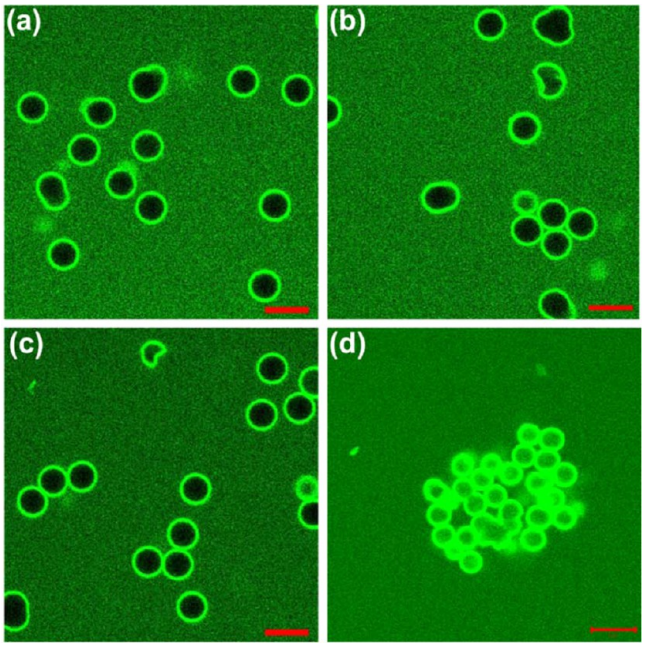

Figure 5. CLSM images of $(PSS/PDMAEMA_{18})_n$ microcapsules prepared from salt solution with 5 bilayers (a), 8 bilayers (b), and 11 bilayers (c). $(PSS/PDMAEMA_{18})_5$ prepared from water solution (d) exposed to FITC-dextran with M_w of 4 kDa at pH 5. Scale bar in each panel is 5 μm.

cannot permeate into the microcapsules, while FITC molecules are able to go through the shell at pH $\leq$ 7 condition. Considering the hydrodynamic diameter of FITC-dextran (4K) is approximately 2.8 nm, and that of FITC is 1.1 nm,[52] the average pore size of the (PSS/PDMAEMA) microcapsules is estimated to be between these two values (around 2 nm). This result is in accordance with a previous study,[24] which also showed that for microcapsules fabricated from salt solution with relatively thicker shells, the mesh size is on the order of a few nanometers.

On the other hand, the $(PSS/PDMAEMA_{18})_5$ microcapsules prepared from pure water solution have much higher permeability; as shown in Figure 5, FITC-dextran with M_w up to 250 kDa (hydrodynamic diameter: 22.9 nm) can still diffuse inside (Figure S3), which means the pore size is in the range of 20−30 nm, which is around 10 times higher than those prepared from 0.1 M NaCl solution. Because of the screening of charges and more compact chain conformation in salt solution, the LbL shell would be thicker and more condensed with smaller mesh size. While in aqueous solution without salt, the polyelectrolytes should assume a stretched conformation due to the electrostatic repulsion between charged arms, thus forming a highly porous interpenetrating network with irregular pores distributed through the entire shell. Another important consequence is that the microcapsules prepared from water solution tend to aggregate easily (Figure 5d), while those from salt solution are well dispersed.

dx.doi.org/10.1021/ma501853c | *Macromolecules* 2014, 47, 7858−7868

Moreover, the average size of the hollow $(PSS/PDMAEMA_{18})_5$ microcapsules prepared from water solution (2.66 ± 0.11 μm) is significantly smaller than those prepared from salt solution (3.65 ± 0.13 μm), which can also be attributed to more rigid chain conformation in the multilayer shell; there are much stronger unbalanced stress within the shell during core dissolution, which would lead to shrinkage of the overall size. The ability to tune the permeability of microcapsules several micrometers in size down to the nanometer scale makes the more robust $(PSS/PDMAEMA_{18})$ microcapsules interesting candidates for many potential applications. Therefore, in the rest of the paper, the microcapsules are all prepared from 0.1 M NaCl polyelectrolyte solution unless specifically stated.

To further investigate the effect of the star architecture on the assembly process, we also measured the thickness and surface morphology of the analogous LbL films on planar substrates (Figure 6). The LbL films from star and linear

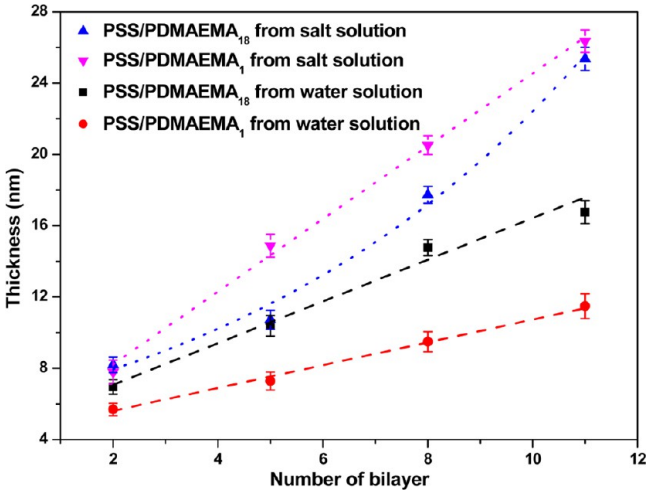

Figure 6. Thickness of PSS/PDMAEMA LbL films as a function of number of bilayers. The dotted lines are fitting from the linear or exponential model.

PDMAEMA in salt solution have very different growth modes: the $PSS/PDMAEMA_{18}$ LbL film exhibits nonlinear growth in thickness, while $PSS/PDMAEMA_1$ LbL film shows conventional linear growth. The nonlinear growth can be attributed to subsurface diffusion, resulting in the increase of film surface roughness with the number of deposited layers.[53] Indeed, AFM images show that the surface of $PSS/PDMAEMA_{18}$ LbL film is highly grainy but uniform without any vermiculate pattern, and the root-mean-square (RMS) roughness is 4.0 nm in a 4 μm^2 area (Figure S4).[54] For $PSS/PDMAEMA_1$ LbL film, the surface is much smoother with RMS roughness of 1.8 nm in a 4 μm^2 area, which indicates the conventional buildup process with alternate overcompensation of the surface charge after each deposition.[55] On the other hand, the LbL films prepared from water solution have linear growth pattern for both star and linear PDMAEMA, and their thickness is much smaller compared with those prepared from salt solution. The absence of charge screening and more stretched conformation prevent the excessive buildup process.

Finally, the $(PSS/PDMAEMA_{18})_8$ and $(PSS/PDMAEMA_1)_8$ microcapsules were exposed to FITC solution at pH 5 with different concentration of NaCl, as shown in Figure 7a,b. It can be seen that $(PSS/PDMAEMA_{18})_8$ microcapsules are stable in high ionic strength condition, while $(PSS/PDMAEMA_1)_8$

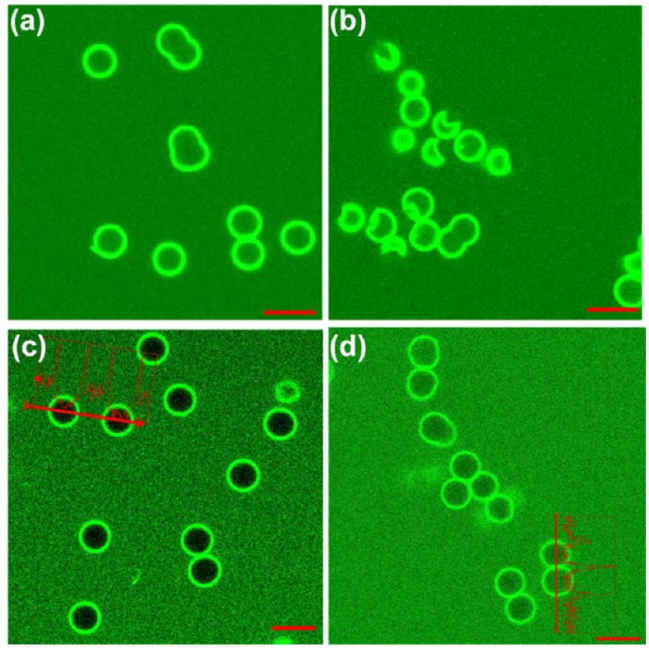

Figure 7. CLSM images of $(PSS/PDMAEMA_{18})_8$ (a) and $(PSS/PDMAEMA_1)_8$ microcapsules (b) exposed to 0.5 M NaCl solution at pH = 5 and FITC added. Permeability of $(PSS/PDMAEMA_{18})_8$ microcapsules in buffer (c) and in 0.5 M NaCl solution (d) to 4 kDa FITC-dextran. The insets are the representative fluorescent intensity profile over the microcapsule. Scale bar in each panel is 5 μm.

microcapsules tend to aggregate and be deformed, which happens to a higher extent with the increase of salt concentration. We suggest that due to the abundance of charged sites on star PDMAEMA chains, they can maintain a relatively highly charged state in spite of the shielding effect compared with the linear counterpart; therefore, the $(PSS/PDMAEMA_{18})_n$ microcapsules are less likely to aggregate.[57] On the other hand, the salt induces polyelectrolyte rearrangements which can result in the formation of local defects on the shell,[62] and the exposure to high salt concentration would lead to an osmotic pressure induced compression. As a result, a significant portion of $(PSS/PDMAEMA_1)_8$ microcapsules are deformed to crescent shape in 0.5 M NaCl solution. Star PDMAEMA has more cross-linking sites with PSS, and the microcapsules have a thicker and stable shell, which makes them more resistant to such kind of deformation.

Ionic strength can also be used to tune the permeability of the star PDMAEMA based microcapsules, as shown in Figure 7c,d. FITC-dextran with 4 kDa is impermeable to $(PSS/PDMAEMA_{18})_8$ microcapsules in 0.01 M Tris-HCl buffer with pH 5, but when the microcapsules were exposed to 0.5 M NaCl solution, they became much more permeable. The reason for which is also due to the salt induced polyelectrolyte rearrangements; the chains become more mobile and local defects can be generated. Because of the higher stability of the star PDMAEMA based LbL microcapsules, in the following study we focus on the $(PSS/PDMAEMA_{18})_n$ microcapsules.

pH Response of $(PSS/PDMAEMA_{18})$ LbL Microcapsules. Taking advantage of the pH-dependent behavior of PDMAEMA, the structure and permeability of the corresponding LbL microcapsules are also expected to change with pH. Indeed, as shown in Figure 8, at pH ≤ 7 conditions, the FITC is able to diffuse into the $(PSS/PDMAEMA_{18})$ microcapsules;

dx.doi.org/10.1021/ma501853c | Macromolecules 2014, 47, 7858−7868

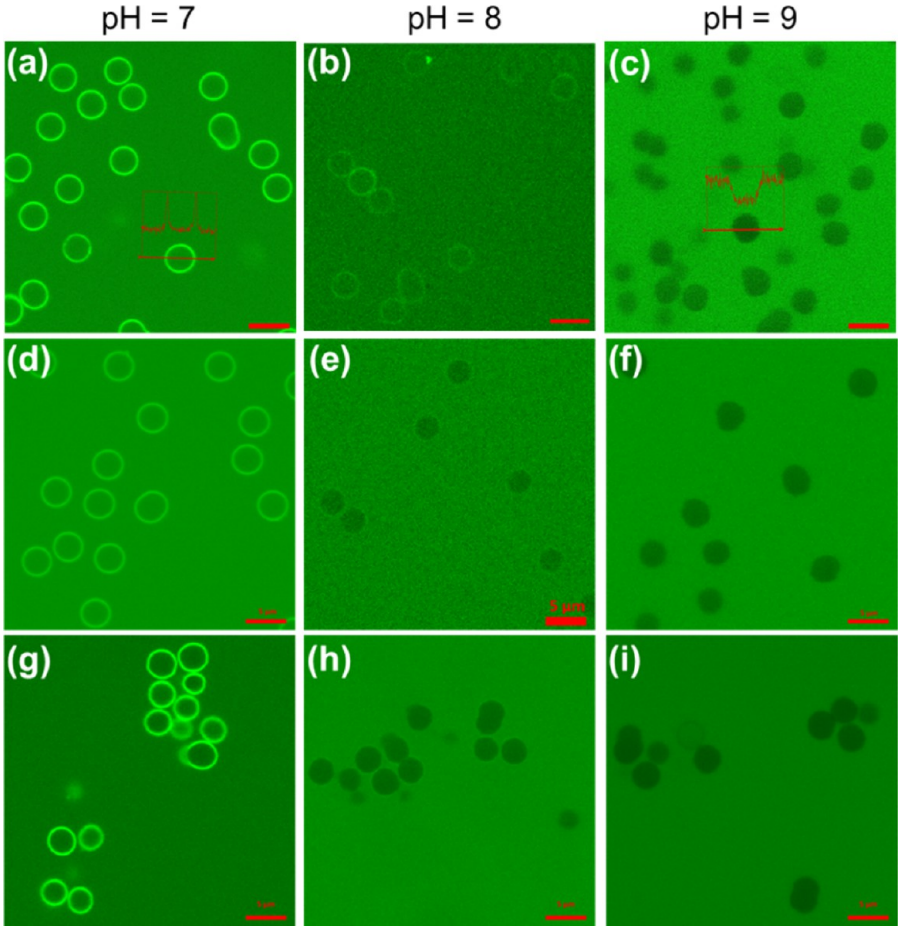

Figure 8. CLSM images of $(PSS/PDMAEMA_{18})_n$ microcapsules with 5 bilayers (a, b, c), 8 bilayers (d, e, f), and 11 bilayers (g, h, i) exposed to FITC solutions at different pH conditions as labeled on each column. The inset in (a) and (c) is the representative fluorescent intensity profile over the microcapsule. Scale bar in each panel is 5 μm.

however, as the pH increases, the permeability of the microcapsules decreases. For $(PSS/PDMAEMA_{18})_5$ microcapsules, the transition from permeable to impermeable state happens at pH 9. While for $(PSS/PDMAEMA_{18})_{11}$ microcapsules, due to the increased shell thickness, the transition already happens at pH 8 for $(PSS/PDMAEMA_{18})_8$ and $(PSS/PDMAEMA_{18})_{11}$.

The permeability test results are summarized in Table 1. For the sake of comparison, we also studied the responsiveness of

Table 1. Permeability of $(PSS/PDMAEMA_{18})_n$ and $(PSS/PDMAEMA_1)_n$ Microcapsules to FITC at Different pH Conditions (+: Permeable; −: Not Permeable)

sample	pH = 3	pH = 5	pH = 7	pH = 8	pH = 9
$(PSS/PDMAEMA_{18})_5$	+	+	+	+	−
$(PSS/PDMAEMA_{18})_8$	+	+	+	−	−
$(PSS/PDMAEMA_{18})_{11}$	+	+	+	−	−

microcapsules based on linear PDMAEMA. As shown in Figure S5, the $(PSS/PDMAEMA_1)_n$ microcapsules show a similar trend of permeability changes with increasing pH.

As known, the electrostatic cross-links within the polyelectrolyte multilayer shell are dynamic and sensitive to pH and electrostatic screening, which allows the chains to undergo certain reorganization due to the breaking and re-forming of ionic cross-links that hold the multilayer shell together.[56] This reorganization process has been found to lead to reversible pore opening or closing in certain weak polyelectrolyte multilayer films.[57] At low pH value, the majority of the free amino groups on PDMAEMA chains are charged, which would cause the chains to extend due to the electrostatic repulsion. As a result, the spacing between the chains in the multilayer system is larger; in other words, the microcapsules have higher permeability, which allows the facile diffusion of FITC.[57] The $(PSS/PDMAEMA_{18})_n$ microcapsules are very stable at acid condition down to pH 1 (Figure S6).

With the increase of pH value, the charge density on PDMAEMA chain dimensions decrease. As a result, the electrostatic repulsion force decreases, which leads to the contraction of the flexible chains. Since the PSS chains are closely bound to PDMAEMA, the contraction of PDMAEMA chains would also force the whole multilayer shell to contract, which results in a denser shell and lower permeability as depicted in Scheme 2.

On the other hand, the density of ionic cross-links also decreases with increasing pH, leading to a more flexible membrane, and possible defects in the microcapsule shell are filled by the more dynamic chains. The critical value for the permeation of FITC molecules is in between pH 8 or 9 depending on the shell thickness (Figure 8). The overall size of the microcapsule also gradually decreases with increasing pH; for example, the average size of $(PSS/PDMAEMA_{18})_8$ microcapsules decreases from 3.65 μm (±0.10) at pH 7 to

dx.doi.org/10.1021/ma501853c | Macromolecules 2014, 47, 7858−7868

Scheme 2. Structural Changes of the $(PSS/PDMAEMA_{18})$ Microcapsules in Response to Different External Stimuli Including Ionic Strength, pH, and Temperature

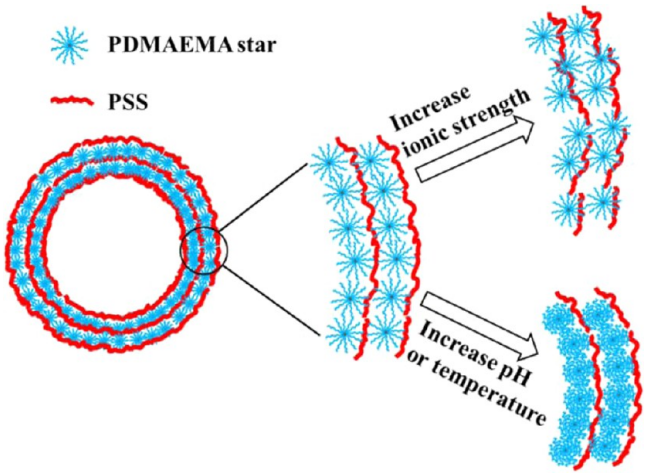

3.33 μm ($\pm$0.12) at pH 9, as measured by CLSM in solution state. The morphology of the microcapsules in dry state from their suspension with different pH values provides additional evidence to the dimensional changes.

As shown in Figure 9, $(PSS/PDMAEMA_{18})_{11}$ microcapsules have relatively thin shell and flat surface at pH 5, and the shell gradually become denser with large wrinkles forming on the surface at pH 7. Eventually, the microcapsules have thick and rigid shell which tends not to collapse during drying, so that the spherical shape is largely retained and the shells are partially broken during drying. At the same time, the size of the microcapsules in dry state also decreases with increasing pH.

If the pH value further increases to above 9, the shell integrity would be compromised and FITC can permeate through the damaged region into the microcapsules. As can be seen from Figure S7, at pH 10 condition about half of the $(PSS/PDMAEMA_{18})_8$ microcapsules are broken and FITC can diffuse inside. With further increase of pH to 11, most of the microcapsules are damaged, and almost no intact spherical microcapsules can be found. The $PSS/PDMAEMA_{18}$ microcapsules have higher stability in such extreme pH conditions compared with $(PSS/PDMAEMA_1)_8$ microcapsules (Figure S7).

Another interesting phenomenon observed in this study is that not only the permeability of target molecules inside the microcapsules can be controlled by pH, but also the incorporation of target molecules into the shell is influenced by pH conditions. It can be seen from Figure 8 that at pH 7 the FITC molecules can be readily absorbed on the shell, which show higher fluorescence intensity than the background. When the pH value increases to 8, less FITC molecules are bound to the shell, and at pH 9 the shell is not visible, which means FITC cannot attach to the shell. FITC is negatively charged in the pH range used for our study, so that they can bind with PDMAEMA chains through electrostatic interaction. When the charge density of PDMAEMA decreases with increasing pH value, the interaction between FITC and PDMAEMA also decreases, resulting in a reduced FTIC absorption.

Taking advantage of the pH responsive permeability of $(PSS/PDMAEMA_{18})_n$ microcapsules, we also performed encapsulation and release of FITC molecules in solution (Figure 10). By exposing the $(PSS/PDMAEMA_{18})_8$ microcapsules to FITC solution at pH 7, the dye molecules can readily permeate inside; then after collecting the microcapsules through centrifugation and replacing the supernatant with pH 9 buffer, the permeability of the microcapsules decreases so that the FITC can be encapsulated with the background dye removed. The encapsulated FITC can be quickly released by exposing the microcapsules to pH 7 buffer again. The encapsulation and release are completely reversible and can be done multiple times with high efficiency (Figure 10).

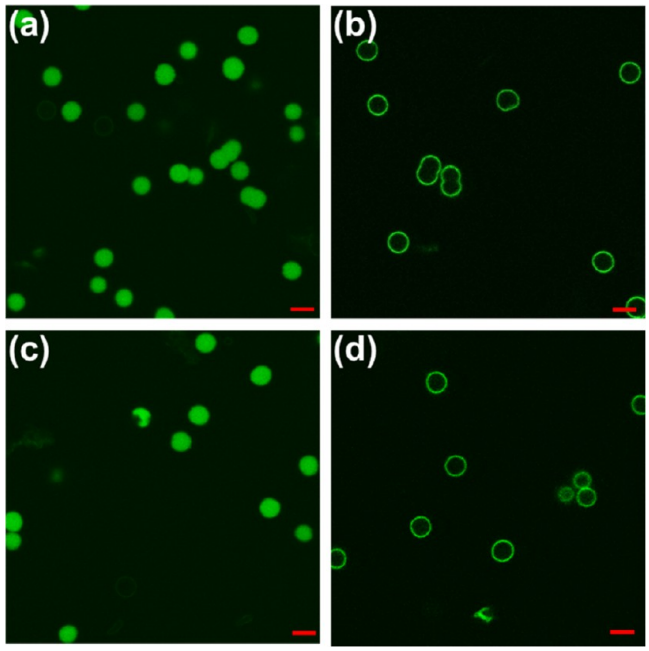

Figure 10. $(PSS/PDMAEMA_{18})_8$ microcapsules encapsulation of FITC at pH 9 (a) and release at pH 7 (b); the second cycle of encapsulation and release (c, d). Scale bar is 5 μm in all images.

Temperature Response of $(PSS/PDMAEMA_{18})$ Microcapsules. PDMAEMA is a well-studied water-soluble thermoresponsive polyelectrolyte, and the cloud points of PDMAEMA solutions strongly decrease with increasing

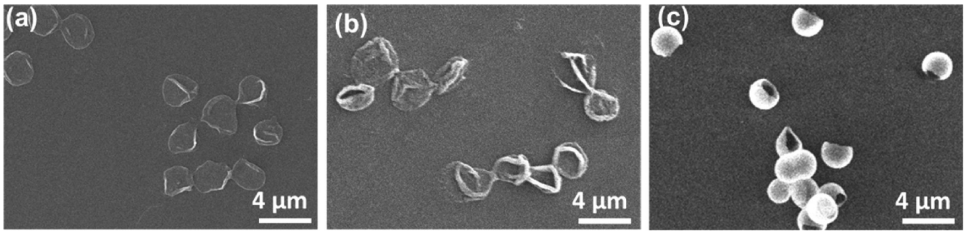

Figure 9. SEM images of $(PSS/PDMAEMA_{18})_{11}$ microcapsules with different pH conditions: (a) pH = 5, (b) pH = 7, and (c) pH = 9.

dx.doi.org/10.1021/ma501853c | Macromolecules 2014, 47, 7858−7868

pH.[47,58] With the increase of temperature, water becomes a bad solvent for PDMAEMA, the hydrogen bonding between PDMAEMA chains and water weakens, and the hydrophobic interaction increases,[59] so that the arms of PDMAEMA stars shrink to a more collapsed conformation,[60] which leads to changes in the structure and permeability of the microcapsule.

As shown in the previous section, the transition of (PSS/$PDMAEMA_{18}$) microcapsules from being permeable to being impermeable to FITC molecules occurs between pH 8 and 9. Therefore, for following study, we chose pH 7 as the condition to load FITC dye molecules inside the microcapsules. The encapsulation was done by incubating the microcapsules in solution containing FITC dye at room temperature. The solution was then transferred to a dialysis tube in pH 7 buffer bath at a preset temperature of 45 °C with constant stirring. Dialysis at 45 °C was continued until the concentration of FITC in the buffer was very low and remained unchanged, as monitored by a fluorophotometer.

Then the whole system was cooled down to a series of preset temperatures (40, 35, 30, 25, and 20 °C) consecutively; at each preset temperature the buffer bath was equilibrated for 15 min, and then the fluorescence intensity of the bath which contains the FITC molecules permeate from the microcapsules was measured. The results are shown in Figure 11a; it can be seen that the intensity of the FITC emission peak of (518 nm) increases as the cooling proceeds.

The results give strong indication that FITC dye was successfully encapsulated and retained inside the microcapsules at 45 °C but can be subsequently released by decreasing the temperature (Figure 11). With the decrease of temperature, the PDMAEMA stars can recover from their collapsed state; therefore, the shell of microcapsules also become more swollen and permeable for FITC. The thermoresponsive encapsulation and release is also completely reversible, as shown in Figure 11b. FITC molecules can be encapsulated inside the microcapsules at 45 °C and be released at 20 °C with high efficiency in a cyclical fashion. Such temperature-induced loading–unloading cycling can be repeated numerous (more than 10) times.

Moreover, it has been found that pH conditions also affect the thermoresponsive behavior of microcapsules, proving direct cross-correlation of two independent stimuli. As shown in Figure S8, when the encapsulation and release are performed at a lower pH condition (pH 6), the encapsulation efficiency somewhat decreases, as indicated by the relative fluorescent intensity changes during cooling at the same condition. The reason for this can be related to the earlier pH responsiveness discussion; basically, at lower pH condition the permeability of PSS/$PDMAEMA_{18}$ microcapsules is higher, so that less amount of FITC molecules can be encapsulated at the same temperature.

The thermoresponsiveness has also been proved by the changes in size and morphology of the microcapsules as measured by AFM. From Figure 12 it can be seen that the average overall size of the dried microcapsules shrink from 4.47 (±0.31) μm at 20 °C, to 3.42 (±0.18) μm at 40 °C, and 2.07 (±0.16) μm at 60 °C. At the same time, the average thickness of the microcapsules increases from 24.8 (±1.1) nm at 20 °C, to 29.4 (±2.6) nm at 40 °C, and 76.0 (±7.9) nm at 60 °C. The significant size reduction and densification of shell caused by changing hydrophobic–hydrophilic balance corroborate the permeability changes of the microcapsules with increasing temperature.

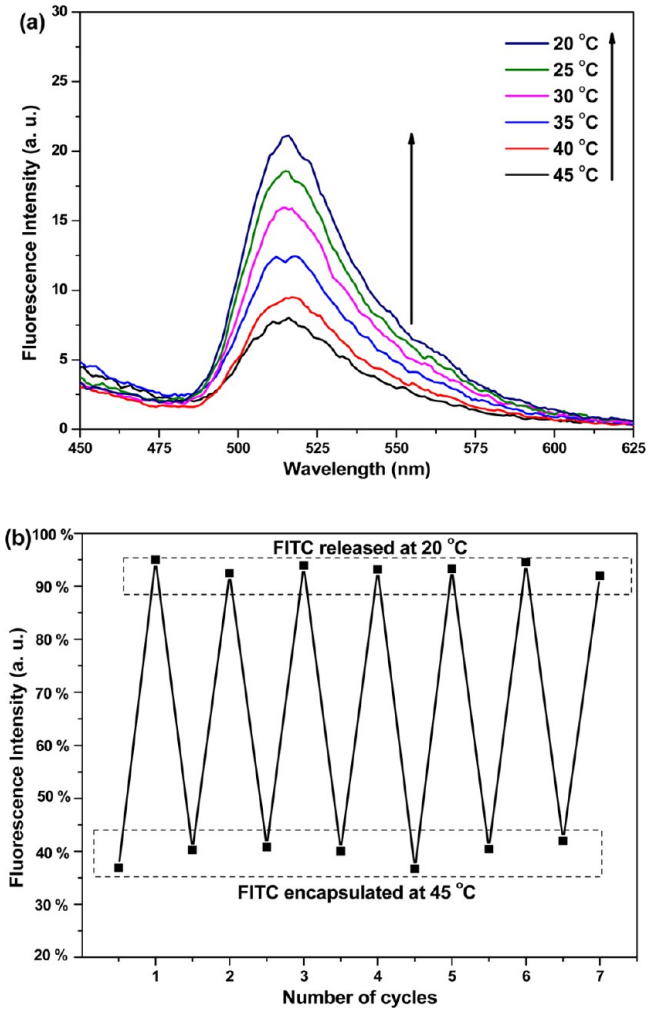

Figure 11. (a) Fluorescence intensity of the dialysis bath which contains the FITC molecules permeate from the microcapsules, during the cooling of $(PSS/PDMAEMA_{18})_8$ microcapsules from 45 to 20 °C. (b) Reversibility of the thermoresponsive encapsulation and release as indicated by fluorescence intensity of the dialysis bath.

Our results of the thermoresponsiveness of microcapsules based on responsive PDMAEMA star polyelectrolyte are unique and superior in certain aspects compared with previous studies on conventional LbL microcapsules. A study on PSS/PAH microcapsules[61] indicates that the capsule size decreases when heated; the density and volume of the microcapsules shell remained approximately constant. But the magnitude of the observed decrease in the former case is much lower compared with our results. In another study the annealing at high temperature (40 °C) even led to the swelling of the microcapsules.[62]

3. CONCLUSIONS

In conclusion, responsive PDMAEMA star polyelectrolytes (to pH and temperature) were successfully used as main component to fabricate LbL microcapsules. The microcapsules are able to respond to multiple external stimuli, such as ionic strength, pH, and temperature. With increasing pH, the permeability of microcapsules decreases, and the transition from "open" to "closed" state for target molecules can be accurately tuned within a narrow pH range. Furthermore, due to the thermoresponsiveness of PDMAEMA stars, the overall

dx.doi.org/10.1021/ma501853c | Macromolecules 2014, 47, 7858–7868

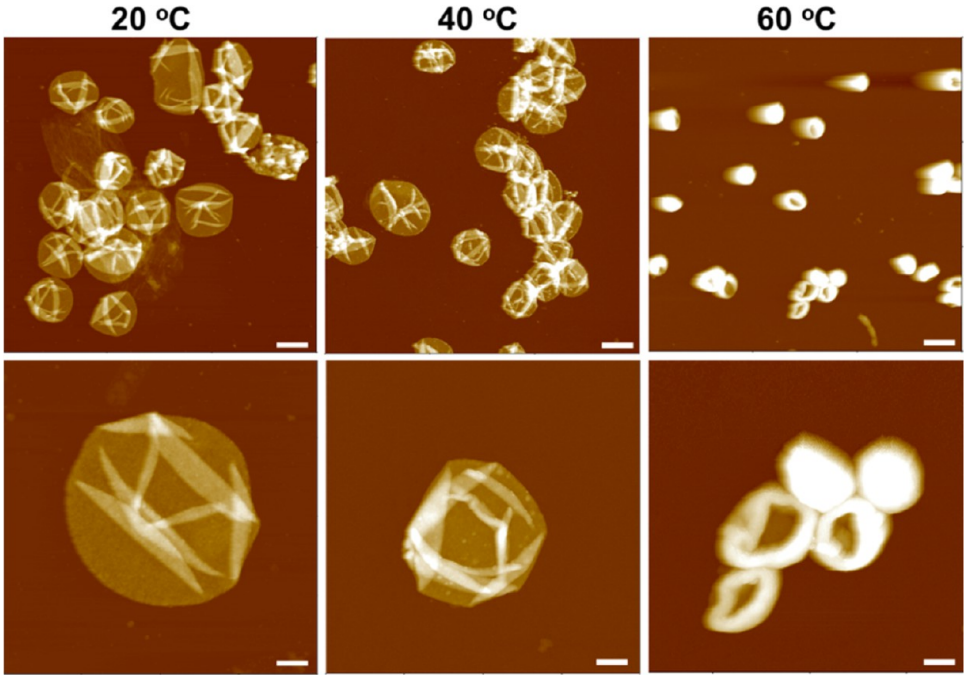

Figure 12. Size and morphology changes of $(PSS/PDMAEMA_{18})_5$ microcapsules with increase of temperature as shown by AFM images. Scale bar is 3 μm for top row and 1 μm for bottom row. Z range is 500 nm for 20 and 40 °C images and 2000 nm for 60 °C images.

size and permeability of the microcapsules decrease with increasing temperature; a reversible encapsulation and release of cargo molecules by temperature changes can be achieved. The organization and interaction of star polyelectrolytes within confined multilayer structure are the main driving forces for the multiple responsive behaviors.

This study is the first demonstration of multiresponsive microcapsules from branched macromolecules and provides insights to the interaction and assembly of star polyelectrolytes in multilayered systems. The microcapsules based on responsive star polyelectrolytes provide a robust and smart platform to enable the controlled loading and unloading of target molecules under multiple stimuli. For example, the star polyelectrolytes can serve as nanocarriers for target molecule I, and target molecule II can be encapsulated in the hollow core region of microcapsules; then by applying different stimuli simultaneously or consecutively, the target molecules can be released in a controlled and logic way, which is superior to most conventional polyelectrolyte microcapsules. Moreover, the ability of the LbL microstructure to translate multiple external stimuli into physical response has the potential to be used as multi-input logic gates and polymer memory devices,[63] which was demonstrated mostly for small molecules or polymers before.

4. EXPERIMENTAL SECTION

Materials. Poly(ethylene imine) (PEI) was purchased from Polysciences. Poly(sodium 4-styrenesulfonate) (PSS, M_w = 70 000 kg/mol) was purchased from Sigma-Aldrich. All commercial polyelectrolytes were used without further purification. Silica particles with a diameter of 4.0 ± 0.2 μm and 10% dispersion in water were obtained from Polysciences. Hydrofluoric acid (48−51%) was purchased from BDH Aristar. Nanopure water (Nanopure system, Barnstead) with a resistivity of 18.2 MΩ cm was used in all experiments. Tris-HCl (1.0 M) was purchased from Rockland and was diluted to 0.01 M in ultrapure pure water with pH adjusted by HCl or NaOH for use.

Synthesis of PDMAEMA Star Polyelectrolytes. PDMAEMA star polymers were synthesized by atom transfer radical polymerization of 2-(*N*,*N*-dimethylamino)ethyl methacrylate employing a core-first route with functionalized polyhedral oligomeric silsesquioxane (POSS) core as described earlier[64] (Scheme 1). Silsesquioxane nanoparticles were used as multifunctional initiators; the rather low efficiency of the initiation sites (30−75%) leads to a moderate arm number distribution of the prepared polyelectrolyte stars. Here, we used PDMAEMA star polymers with 18 arms, with the number-average degree of polymerization (DP) per arm of 170, M_n of 910 kDa, and a (polydispersity index) PDI of 1.2. The linear PDMAEMA used in this study for comparative purposes has a DP of 450, M_n of 28.8 kDa, and a PDI of 1.98.

Preparation of LbL Microcapsules and Films. PSS and PDMAEMA star polyelectrolyte were each dissolved in 0.1 M NaCl solution with the concentration of 0.2 mg/mL. PEI solution (1.0 mg/mL) in Nanopure water was used to deposit the prelayer. The preparation of LbL $(PSS/PDMAEMA)_n$ microcapsules is shown in Scheme 1b: the bare, negatively charged silica particles with average diameter of 4.0 μm were first coated with a PEI prelayer by incubating in 1.5 mL of PEI solution (1.0 mg/mL) for 15 min, followed by two centrifugation (3000 rpm for 3 min)/wash cycles. Subsequently, the silica particles were incubated in 1.5 mL PSS solution (0.2 mg/mL) for 15 min, followed by two centrifugation (3000 rpm for 3 min)/wash cycles. 1.5 mL of PDMAEMA star polyelectrolyte solution was then added, and 15 min was allowed for adsorption, also followed by two centrifugation/wash cycles. The adsorption steps were repeated until the desired number of layers was built on silica particles. Hollow microcapsules were finally obtained by dissolving silica cores in 1% HF solution for 2 h, followed by dialysis in Nanopure water for 2 days with repeated change of water. The LbL films were prepared by the dip-assisted LbL method: the silicon substrate was alternately immersed in PSS and PDMAEMA polyelectrolyte solution for 15 min, followed by two times rinsing with water or 0.01 M Tris-HCl buffer.

Atomic Force Microscopy (AFM). AFM images were obtained using a Dimension-3000 (Digital Instruments) microscope in the "light" tapping mode according to the well-established procedure.[65] Silicon wafers were cleaned with piranha solution (3:1 concentrated sulfuric acid and hydrogen peroxide mixture; *caution: strong oxidizer!*) according to the known procedure.[66] Then wafers were rinsed

dx.doi.org/10.1021/ma501853c | *Macromolecules* 2014, 47, 7858−7868

thoroughly with Nanopure water and dried with a nitrogen stream. For sample preparation, a drop of microcapsule suspension was placed onto a precleaned silicon wafer and dried in air prior to AFM imaging. Thickness of the microcapsules was determined as half of the height of the collapsed flat regions of dried microcapsules from height histograms by NanoScope software.[67]

Scanning Electron Microscopy (SEM). SEM imaging of hollow microcapsules was performed on a Hitachi S-3400-II scanning electron microscope with electric current of 10 kV in a vacuum (<1 Pa). Microcapsules were air-dried on silicon wafers and sputter-coated with gold before imaging.

Transmission Electron Microscopy (TEM). TEM was done using a JEOL 100CX operated at 100 kV with samples drop-cast on carbon−Formvar-coated copper grids (Ted Pella, Inc.).

Zeta-Potential Measurements. Surface potentials of bare and coated silica particles were measured from aqueous solutions on Zetasizer Nano-ZS equipment (Malvern), and the ζ-potential was obtained using the Smoluchowski relation. Each value of the zeta-potential was obtained at ambient conditions by averaging three independent measurements of 35 subruns each.

Confocal Laser Scanning Microscopy (CLSM). Confocal images of microcapsules were obtained with an LSM 510 UV Vis laser scanning microscope (Zeiss, Germany) equipped with C-Apochromat 63× oil immersion objective. The excitation/emission wavelengths were 488/515 nm. Microcapsules were visualized through addition of fluorescein isothiocyanate (FITC) to the solution. A drop of hollow microcapsule suspension was added to Lab-Tek chamber (Electron Microscopy Sciences), which was then filled with water or buffer with microcapsules allowed to settle down.

■ ASSOCIATED CONTENT

Ⓢ Supporting Information

AFM and confocal microscopy images of the LbL microcapsules as well as thin films are included. This material is available free of charge via the Internet at http://pubs.acs.org.

■ AUTHOR INFORMATION

Corresponding Author

*E-mail: vladimir@mse.gatech.edu (V.V.T.).

Present Addresses

F.A.P.: Institute of Physical Chemistry, RWTH Aachen University, 52056 Aachen, Germany.

A.H.E.M.: Institute of Organic Chemistry, University of Mainz, 55099 Mainz, Germany.

Notes

The authors declare no competing financial interest.

■ ACKNOWLEDGMENTS

This work is supported by Grant NSF-DMR 1002810. The authors are grateful to Dr. Ikjun Choi for the helpful discussions during the early stage of the study.

■ REFERENCES

(1) Stuart, M. A. C.; Huck, W. T.; Genzer, J.; Müller, M.; Ober, C.; Stamm, M.; Sukhorukov, G. B.; Szleifer, I.; Tsukruk, V. V.; Urban, M.; Winnik, F.; Zauscher, S.; Luzinov, I.; Minko, S. *Nat. Mater.* **2010**, *9*, 101−113.

(2) Luzinov, I.; Minko, S.; Tsukruk, V. V. *Soft Matter* **2008**, *4*, 714−725.

(3) Santer, S.; Kopyshev, A.; Donges, J.; Yang, H. K.; Ruhe, J. *Adv. Mater.* **2006**, *18*, 2359−2362.

(4) Hendrikson, G. R.; Lyon, L. A. *Soft Matter* **2009**, *5*, 29−35.

(5) Synatschke, C. V.; Nomoto, T.; Cabral, H.; Förtsch, M.; Toh, K.; Matsumoto, Y.; Miyazaki, K.; Hanisch, A.; Schacher, F. H.; Kishimura, A.; Nishiyama, N.; Müller, A. H. E.; Kataoka, K. *ACS Nano* **2014**, *8*, 1161−1172.

(6) Steinschulte, A.; Schulte, B.; Rütten, S.; Eckert, T.; Okuda, J.; Möller, M.; Schneider, S.; Borisov, O. V.; Plamper, F. A. *Phys. Chem. Chem. Phys.* **2014**, *16*, 4917−4932.

(7) Lu, Y.; Mei, Y.; Drechsler, M.; Ballauff, M. *Angew. Chem., Int. Ed.* **2006**, *45*, 813−816.

(8) Plamper, F. A.; Gelissen, A. P.; Timper, J.; Wolf, A.; Zezin, A. B.; Richtering, W.; Tenhu, H.; Simon, U.; Mayer, J.; Borisov, O. V.; Pergushov, D. V. *Macromol. Rapid Commun.* **2013**, *34*, 855−860.

(9) Chia, K.; Rubner, M. F.; Cohen, R. E. *Langmuir* **2009**, *25*, 14044−14052.

(10) Johnston, A. P. R.; Cortez, C.; Angelatos, A. S.; Caruso, F. *Curr. Opin. Colloid Interface Sci.* **2006**, *11*, 203−209.

(11) Ionov, L. *Adv. Funct. Mater.* **2013**, *23*, 4555−4570.

(12) Drachuk, I.; Shchepelina, O.; Lisunova, M.; Harbaugh, S.; Kelley-Loughnane, N.; Stone, M.; Tsukruk, V. V. *ACS Nano* **2012**, *6*, 4266−4278.

(13) Fakhrullin, R. F.; Lvov, Y. M. *ACS Nano* **2012**, *6*, 4557−4564.

(14) Wang, Y.; Hosta-Rigau, L.; Lomas, H.; Caruso, F. *Phys. Chem. Chem. Phys.* **2011**, *13*, 4782−4801.

(15) De Cock, L. J.; De Koker, S.; De Geest, B. G.; Grooten, J.; Vervaet, C.; Remon, J. P.; Sukhorukov, G. B.; Antipina, M. N. *Angew. Chem., Int. Ed.* **2010**, *49*, 6954−6973.

(16) Ariga, K.; Hill, J. P.; Ji, Q. *Phys. Chem. Chem. Phys.* **2007**, *9*, 2319−2340.

(17) Fery, A.; Tsukruk, V. V. In *Multilayer Thin Films: Sequential Assembly of Nanocomposite Materials*, 2nd ed.; Decher, G., Schlenoff, J., Eds.; Wiley-VCH: Weinheim, Germany, 2012; Vol. *1*.

(18) Jiang, C.; Tsukruk, V. V. *Adv. Mater.* **2006**, *18*, 829−840.

(19) De Geest, B. G.; Sanders, N. N.; Sukhorukov, G. B.; Demeester, J.; De Smedt, S. C. *Chem. Soc. Rev.* **2007**, *36*, 636−649.

(20) Sukhishvili, S. A. *Curr. Opin. Colloid Interface Sci.* **2005**, *10*, 37−44.

(21) Ye, C.; Shchepelina, O.; Calabrese, R.; Drachuk, I.; Kaplan, D. L.; Tsukruk, V. V. *Biomacromolecules* **2011**, *12*, 4319−4325.

(22) Yi, Q.; Wen, D.; Sukhorukov, G. B. *Langmuir* **2012**, *28*, 10822−10829.

(23) Hoy, O.; Zdyrko, B.; Lupitskyy, R.; Sheparovych, R.; Aulich, D.; Wang, J.; Bittrich, E.; Eichhorn, K.; Uhlmann, P.; Hinrichs, K.; Müller, M.; Stamm, M.; Minko, S.; Luzinov, I. *Adv. Funct. Mater.* **2010**, *20*, 2240−2247.

(24) Dong, W. F.; Ferri, J. K.; Adalsteinsson, T.; Schönhoff, M.; Sukhorukov, G. B.; Möhwald, H. *Chem. Mater.* **2005**, *17*, 2603−2611.

(25) Bedard, M. F.; De Geest, B. G.; Skirtach, A. G.; Mohwald, H.; Sukhorukov, G. B. *Adv. Colloid Interface Sci.* **2010**, *158*, 2−14.

(26) Borges, J.; Rodrigues, L. C.; Reis, R. L.; Mano, J. F. *Adv. Funct. Mater.* **2014**, DOI: 10.1002/adfm.201401050.

(27) Xu, W.; Choi, I.; Plamper, F. A.; Synatschke, C. V.; Müller, A. H. E; Tsukruk, V. V. *ACS Nano* **2013**, *7*, 598−613.

(28) Lu, Z. H.; Prouty, M. D.; Guo, Z. H.; Golub, V. O.; Kumar, C.; Lvov, Y. M. *Langmuir* **2005**, *21*, 2042−2050.

(29) Plamper, F. A. *Adv. Polym. Sci.* **2014**, DOI: 10.1007/1012_2014_1284.

(30) Zahn, R.; Voros, J.; Zambelli, T. *Curr. Opin. Colloid Interface Sci.* **2010**, *15*, 427−434.

(31) Skirtach, A. G.; De Geest, B. G.; Mamedov, A.; Antipov, A. A.; Kotov, N. A.; Sukhorukov, G. B. *J. Mater. Chem.* **2007**, *17*, 1050−1054.

(32) Xu, L.; Zhu, Z.; Sukhishvili, S. *Langmuir* **2011**, *27*, 409−415.

(33) Bedard, M. F.; Munoz-Javier, A.; Mueller, R.; del Pino, P.; Fery, A.; Parak, W. J.; Skirtach, A. G.; Sukhorukov, G. B. *Soft Matter* **2009**, *5*, 148−155.

(34) Kozlovskaya, V.; Kharlampieva, E.; Drachuk, I.; Cheng, D.; Tsukruk, V. V. *Soft Matter* **2010**, *6*, 3596−3608.

(35) Kuroki, H.; Tokarev, I.; Nykypanchuk, D.; Zhulina, E.; Minko, S. *Adv. Funct. Mater.* **2013**, *23*, 4593−4600.

(36) Kowalczuk, A.; Trzcinska, R.; Trzebicka, B.; Dworak, A.; Müller, A. H. E.; Tsvetanov, C. B. *Prog. Polym. Sci.* **2014**, *39*, 43−86.

(37) Yang, W. C.; Xie, R.; Pang, X. Q.; Ju, X. J.; Chu, L. Y. *J. Membr. Sci.* **2008**, *321*, 324−330.

(38) Wang, Z.; Feng, Z.; Gao, C. *Chem. Mater.* **2008**, *20*, 4194−4199.

(39) Berger, S.; Zhang, H.; Pich, A. *Adv. Funct. Mater.* **2009**, *19*, 554−559.
(40) Gao, H.; Matyjaszewski, K. *Prog. Polym. Sci.* **2009**, *34*, 317−392.
(41) Peleshanko, S.; Tsukruk, V. V. *J. Polym. Sci., Part B: Polym. Phys.* **2012**, *50*, 83−100.
(42) Peleshanko, S.; Tsukruk, V. V. *Prog. Polym. Sci.* **2008**, *33*, 523−580.
(43) Jia, P. T.; Argun, A. A.; Xu, J. W.; Xiong, S. X.; Ma, J.; Hammond, P. T.; Lu, X. H. *Chem. Mater.* **2010**, *22*, 6085−6091.
(44) Kim, B. S.; Gao, H. F.; Argun, A. A.; Matyjaszewski, K.; Hammond, P. T. *Macromolecules* **2009**, *42*, 368−375.
(45) Choi, I.; Malak, S. T.; Xu, W.; Heller, W. T.; Tsitsilianis, C.; Tsukruk, V. V. *Macromolecules* **2013**, *46*, 1425−1436.
(46) Majewski, A. P.; Stahlschmidt, U.; Jérôme, V.; Freitag, R.; Müller, A. H. E.; Schmalz, H. *Biomacromolecules* **2013**, *14*, 3081−3090.
(47) Plamper, F. A.; Ruppel, M.; Schmalz, A.; Borisov, O.; Ballauff, M.; Müller, A. H. E. *Macromolecules* **2007**, *40*, 8361−8366.
(48) Déjugnat, C.; Sukhorukov, G. B. *Langmuir* **2004**, *20*, 7265−7269.
(49) Tong, W.; Gao, C.; Möhwald, H. *Macromolecules* **2006**, *39*, 335−340.
(50) Lvov, Y.; Antipov, A. A.; Mamedov, A.; Möhwald, H.; Sukhorukov, G. B. *Nano Lett.* **2001**, *1*, 125−128.
(51) Gelissen, A. P. H.; Schmid, A. J.; Plamper, F. A.; Pergushov, D. V.; Richtering, W. *Polymer* **2014**, *55*, 1991−1999.
(52) Yuan, W.; Lv, Y.; Zeng, M.; Fu, B. M. *Microvasc. Res.* **2009**, *77*, 166−173.
(53) Choi, I.; Suntivich, R.; Plamper, F. A.; Synatschke, C. V.; Müller, A. H. E.; Tsukruk, V. V. *J. Am. Chem. Soc.* **2011**, *133*, 9592−9606.
(54) Lavalle, P.; Gergely, C. F.; Cuisinier, J. G.; Decher, G.; Schaaf, P.; Voegel, J. C.; Picart, C. *Macromolecules* **2002**, *35*, 4458−4465.
(55) Picart, C.; Lavalle, P.; Hubert, P.; Cuisinier, F. J. G.; Decher, G.; Schaaf, P.; Voegel, J. C. *Langmuir* **2001**, *17*, 7414−7424.
(56) Burke, S. E.; Barrett, C. J. *Macromolecules* **2004**, *37*, 5375−5384.
(57) Chung, A. J.; Rubner, M. F. *Langmuir* **2002**, *18*, 1176−1183.
(58) Arslan, H.; Pfaff, A.; Lu, Y.; Stepánek, P.; Müller, A. H. E. *Macromol. Biosci.* **2014**, *14*, 81−91.
(59) Thavanesan, T.; Herbert, C.; Plamper, F. A. *Langmuir* **2014**, *30*, 5609−5619.
(60) Yuan, W.; Zou, H.; Guo, W.; Wang, A.; Ren, J. *J. Mater. Chem.* **2012**, *22*, 24783−24791.
(61) Leporatti, S.; Gao, C.; Voigt, A.; Donath, E.; Möhwald, H. *Eur. Phys. J. E* **2001**, *5*, 13−20.
(62) Gao, C.; Leporatti, S.; Moya, S.; Donath, E.; Möhwald, H. *Chem.—Eur. J.* **2003**, *9*, 915−920.
(63) Dimitrov, I.; Trzebicka, B.; Müller, A. H. E.; Dworak, A.; Tsvetanov, C. B. *Prog. Polym. Sci.* **2007**, *32*, 1275−1343.
(64) Plamper, F. A.; Schmalz, A.; Penott-Chang, E.; Drechsler, M.; Jusufi, A.; Ballauff, M.; Müller, A. H. E. *Macromolecules* **2007**, *40*, 5689−5697.
(65) McConney, M. E.; Singamaneni, S.; Tsukruk, V. V. *Polym. Rev.* **2010**, *50*, 235−286.
(66) Sheller, N. B.; Petrash, S.; Foster, M. D.; Tsukruk, V. V. *Langmuir* **1998**, *14*, 4535−4544.
(67) Elsner, N.; Dubreuil, F.; Fery, A. *Phys. Rev. E: Stat., Nonlinear, Soft Matter Phys.* **2004**, *69*, 031802.